

The determination of the spin and parity of a vector-vector system

Liupan An,¹ Ronan McNulty,² and Mikhail Mikhasenko^{3,*}

¹*School of Physics, Peking University, Beijing, China*

²*School of Physics, University College Dublin, Dublin 4, Ireland*

³*Ruhr University Bochum, Universitätsstraße 150, Bochum, Germany*

(Dated: April 18, 2024)

We present a construction of the reaction amplitude for the inclusive production of a resonance decaying to a pair of identical vector particles such as $J/\psi J/\psi$, $\rho\rho$, $\phi\phi$. The method provides the possibility of determining the spin and parity of a resonance in a model-independent way. The methodology is demonstrated using the Standard Model decay of the Higgs boson to four leptons and through angular correlations in the production and decays of J/ψ pairs.

I. INTRODUCTION

The formation of hadronic matter is one of the few poorly understood parts of Quantum Chromodynamics (QCD). The quark model (QM) [1, 2] works well in classifying conventional hadronic states into mesons and baryons built from the constituent quarks bound in the confined potential. Hadrons beyond conventional mesons and baryons, such as glueballs, hybrid states, and multi-quark states, are referred to as exotic hadrons [3, 4]. They are allowed by the QM, however they have not been seen experimentally until recently [5, 6]. Over the last decade, overwhelming evidence has accumulated for exotic hadrons including tetraquarks, pentaquarks and hadronic molecules in the heavy quarkonium system [7–10], and beyond [11–17]. Despite the large progress in the field, the overall picture and the categorisation of these states remain unclear.

While the quark content of the exotic state is often straightforwardly determined from its decay channel, the quantum numbers are rarely learned in a simple analysis of the mass spectrum. The spin and parity of a resonance are usually found from angular correlations of the decaying particles. One approach to relating such correlations to properties of particles is to derive the reaction matrix element from the interaction terms in the Lagrangian. For non-perturbative interaction of hadrons, an alternative technique is required. We explore the approach that relies on the fundamental constraints and symmetries appurtenant to the strong-interaction theory with no assumption on the underlying dynamics. The reaction amplitude is built using the helicity formalism [18], where the functional form of the matrix element follows from the rotational properties of the decaying particle. The two key constraints that determine the decay properties are parity conservation and permutation symmetry.

In this paper, we provide a practical implementation of the helicity formalism to determine the spin-parity for a system of two identical vector bosons that decay to a pair of leptons or a pair of scalar particles. Amongst its many

applications, we note three in particular. First, it facilitates studies of the $J/\psi J/\psi$ system, where resonance-like structures were reported by the LHCb experiment [13] and confirmed by both the ATLAS [19] and CMS [20] experiments. In none of the three analyses is the interpretation of the $J/\psi J/\psi$ spectrum unambiguously determined. The spectrum shows a broad structure above the $J/\psi J/\psi$ threshold, followed by a resonance-like peak with a dip in between. This can variously be described as multiple resonances or interference between resonant and non-resonant components, and could have contributions from partially reconstructed decays of heavier state. An angular analysis can help to distinguish different scenarios [21–24] and knowledge of the quantum numbers of the states can elucidate the mechanism for the binding of four charm quarks [25–29].

The second application is the investigations of the central exclusive production (CEP) of vector-meson pairs. The colour-free gluon-rich production mechanism of CEP makes the $\rho\rho$ [30–32] and $\phi\phi$ [33, 34] channels particularly suited to searches for glueballs. The helicity approach has been used before to analyse the $\phi\phi$ system decaying to four pseudoscalar particles by several authors [35, 36]. Our method generalizes these ideas and provides an expression for the decay rate as a function of decay angles for a particle with arbitrary spin. It paves the way for a complete partial-wave analysis of the high statistics CEP of four scalar mesons that should be possible with modern LHC data.

The third study-case is the decay of Higgs to two Z bosons and their subsequent decay into four leptons. This final state has been extensively studied in the past as the golden decay mode of the Higgs boson and in searches for physics beyond the Standard Model [37–41]. We use this decay to validate the methodology and as an example of application of statistical methods to distinguish between different spin-parity hypotheses.

We consider the decay $X \rightarrow V(l^+l^-)V(l^+l^-)$ in the rest of this paper. Modifications needed for vector decays to scalars $X \rightarrow V(S^+S^-)V(S^+S^-)$ are given in Appendix A. The paper is organized as follows. The theoretical formalism is presented in Sec. II, split into three parts that deal with: the construction of the general reaction amplitude using the helicity formalism; the

*e-mail: mikhail.mikhasenko@cern.ch

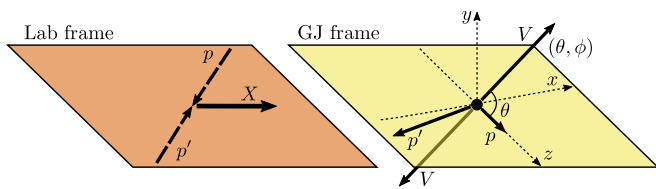


FIG. 1: Schematic view of the production kinematics of the X state in pp collisions. The Gottfried-Jackson frame is used: the axes are defined in the rest frame of X by the vectors of the beam particles: $\vec{z} = \vec{p}/|\vec{p}|$, $\vec{y} = \vec{p}' \times \vec{p}/|\vec{p}' \times \vec{p}|$, $\vec{x} = \vec{y} \times \vec{z}$. The spherical angles (θ, ϕ) are the angles of one of the two decay vectors in the GJ frame. The black arrows shows the three-vectors of the particles. The three-momenta of the vector mesons are labeled by V .

implementation of symmetry constraints; and the discussion of angular moments that can be experimentally observed. This is followed by two applications of these equations in Sec. III: the Higgs decay as an example of an isolated resonance and the $J/\psi J/\psi$ system as a more complicated case. Conclusions follow in Sec. IV.

II. FORMALISM

A. Angular amplitude

We focus on the inclusive production process $pp' \rightarrow X + \dots$, where X is a resonance decaying to two vector mesons. Although the vector mesons are identical, it is convenient to distinguish them in the reaction amplitude calling them V_1 and V_2 . In that way, we can make sure that the amplitude is symmetric under the permutation of indices 1 and 2. When the decay modes of the two vectors are identical, namely $X \rightarrow V(l_1^+ l_1^-) V(l_2^+ l_2^-)$, one needs to account for the symmetrized process $X \rightarrow V(l_1^+ l_2^-) V(l_1^+ l_2^-)$ and the interference between the two decay chains. For narrow resonances, the interference is minor and is neglected in the following discussion. The calculation of interference effects lies beyond the scope of this paper.

The production frame is set up in the rest frame of X as a plane that contains the three-vectors of the production reaction, i.e. \vec{p} and \vec{p}' . The normal to the plane gives the y axis ($\vec{p}' \times \vec{p}$) as shown in Fig. 1. The Gottfried-Jackson (GJ) frame is used to define the x and z axes in the production plane [42], where the z axis is defined along the direction of \vec{p} . The choice of x and z axes is not unique: two other common definitions of the production frame are the helicity (HX) frame, where the z axis is defined by the direction of motion of X itself in the lab frame [18], and the Collins-Soper (CS) frame in which z is defined by the bisector of the angle between \vec{p} and \vec{p}' [43]. We note that a negligibly small polarization is measured in the prompt production of charmonium ("head on" collisions) [44–48]. In contrast, for peripheral processes, e.g. central exclusive production, a significant polarization is

expected [49]. Therefore we consider the general case of an arbitrary polarization of X .

The full kinematics of the decay is described by six angles: a pair of spherical angles $\Omega = (\theta, \phi)$ of the momentum of V_1 in the GJ frame, and two pairs of spherical angles $\Omega_i = (\theta_i, \phi_i)$, $i = 1, 2$ for the decays of the vector mesons V_i in their own HX frames, as illustrated in Fig. 2. The coordinate system for the second vector meson is obtained by the rotation by π about the y axis, followed by a rotation by π about the z axis. The angles ϕ_i can also be defined in the X rest frame as shown in Fig. 2 since they are not affected by the boosts along the vector-meson directions of momentum. The spin of the decay particle X defines the rotational properties of the system of decay products [50]. Every configuration of the three-momenta of the final-state particles in the X rest frame can be considered as a solid body for which the orientation is described by three angles: the pair of spherical angles (θ, ϕ) that describe the direction of \vec{p}_{V_1} , and ϕ_1 , the azimuthal direction of l^+ (see Fig. 1 and Fig. 2). The normalized differential cross section, denoted by the intensity I , reads:

$$I(\Omega, \Omega_1, \Omega_2) = \sum_J (2J+1) \sum_{M, M'} R_{M, M'} \quad (1)$$

$$\times \sum_{\nu, \nu'} D_{M, \nu}^{J*}(\phi, \theta, \phi_1) D_{M', \nu'}^J(\phi, \theta, \phi_1)$$

$$\times \sum_{\xi_1, \xi_2}^{\{-1, 1\}} A_{\xi_1, \xi_2}^{J; \nu}(\theta_1, \theta_2, \Delta\phi) A_{\xi_1, \xi_2}^{J; \nu'*}(\theta_1, \theta_2, \Delta\phi),$$

where the production and decay parts of the amplitude are explicitly separated. The spin of X is denoted by J and M is its spin projection onto the z axis. The definition of the Wigner D-function can be found in Ref. [43]. The production dynamics are encapsulated in the polarization matrix $R_{M, M'}$. The decay amplitude is denoted by A_{ξ_1, ξ_2}^{ν} , where ν is the difference of the vector-meson's helicities, $-2 \leq \nu \leq 2$, and ξ_i is the difference of the two leptons' helicities in the decay of V_i , $-1 \leq \xi_i \leq 1$, $i = 1, 2$. As $\xi_i = 0$ is suppressed by m_l/m_V for the electromagnetic transition, we omit it in the summation. The remaining $V \rightarrow l^+ l^-$ helicity couplings give an overall constant. The decay amplitude is described by the remaining three angles, θ_1 , θ_2 , and $\Delta\phi = \phi_2 + \phi_1$ (see Fig. 2), and is given by

$$A_{\xi_1, \xi_2}^{J; \nu}(\theta_1, \theta_2, \Delta\phi) = \quad (2)$$

$$\frac{3}{2} \sum_{\lambda_1, \lambda_2} \delta_{\nu, \lambda_1 - \lambda_2} H_{\lambda_1 \lambda_2}^J d_{\lambda_1, \xi_1}^1(\theta_1) d_{\lambda_2, \xi_2}^1(\theta_2) e^{i\lambda_2 \Delta\phi}.$$

where λ_1 and λ_2 denote the helicities of the two vector mesons. The phase factor contains only the λ_2 value due to the choice of the reference frame. Once the phase is factored out of the helicity coupling matrix H_{λ_1, λ_2} , the symmetry relations for H are significantly simpler as presented in the next section.

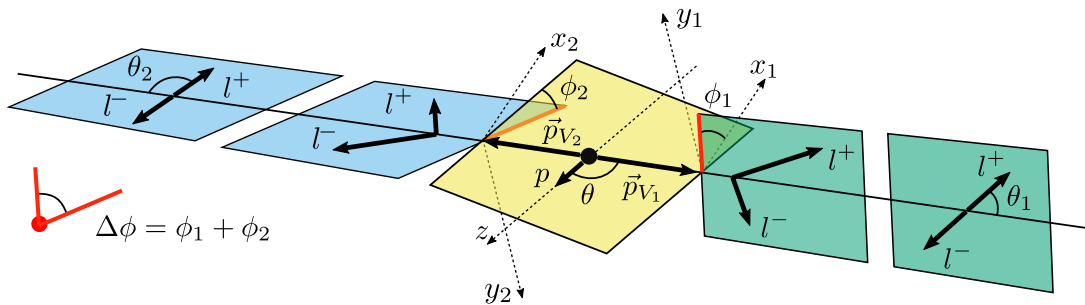


FIG. 2: Schematic view of the $X \rightarrow V(l^+l^-)V(l^+l^-)$ decay kinematics. The central three planes show the orientation of the vector mesons in the X rest frame. The rightmost plane shows the helicity angle θ_1 for the V_1 decay in the rest frame of the two leptons while the leftmost plane shows the helicity for the V_2 decay in the rest frame of the other pair of leptons. The x_1, y_1 and x_2, y_2 axes indicate the directions with respect to which the azimuthal angles of the positive leptons are measured in the decays of the first and second vector, respectively. Both x_1 and x_2 belong to the central yellow plane, both y_1 and y_2 are orthogonal to it.

B. Symmetry constraints

The matrix of the helicity couplings is strictly defined by

$$H_{\lambda_1, \lambda_2} = \langle JM; \lambda_1, \lambda_2 | \hat{T} | JM \rangle, \quad (3)$$

where the bra-state is the projected two-particle state in the particle-2 phase convention, the ket-state is the decaying state with the defined J and M in the GJ frame, and T is the interaction operator [51, 52]. For brevity of notation we omit the index J from the helicity matrix. The following equations constrain the helicity couplings for specific J^P sector. The matrix is constrained by parity and permutation symmetry. Parity transformation relates the opposite values of the vectors' helicities:

$$H_{\lambda_1, \lambda_2} = P(-1)^J H_{-\lambda_1, -\lambda_2}, \quad (4)$$

with P being the internal parity of X . The fact that the two vector mesons are identical relates the helicity matrix with the transposed one:

$$H_{\lambda_1, \lambda_2} = (-1)^J H_{\lambda_2, \lambda_1}. \quad (5)$$

The matrices of the helicity couplings are symmetric (anti-symmetric) for even (odd) spin J . The relations in Eq. (4) and Eq. (5) greatly reduce the number of free components of the helicity matrix, which can in general be written as

$$H = \begin{pmatrix} b & a & c \\ sa & d & \epsilon sa \\ sc & \epsilon a & \epsilon b \end{pmatrix} \quad (6)$$

where a, b, c , and d are the helicity couplings, $\epsilon = P(-1)^J$ is the naturality of X , and the signum, determined by whether the spin of X is odd or even, is given by $s = (-1)^J$. The value of b is non-zero only for positive s , while non-zero d requires both s and ϵ to be positive. According to the values of ϵ and s , all possible quantum

numbers J^P are split into four groups as shown in Table I. The helicity matrix for each groups is

$$I \Rightarrow \begin{pmatrix} b & a & c \\ a & d & a \\ c & a & b \end{pmatrix}, \quad II \Rightarrow \begin{pmatrix} b & a & \\ a & & -a \\ & -a & -b \end{pmatrix}, \quad (7)$$

$$III \Rightarrow \begin{pmatrix} & a & \\ -a & & -a \\ & a & \end{pmatrix}, \quad IV \Rightarrow \begin{pmatrix} & a & c \\ -a & & a \\ -c & -a & \end{pmatrix}. \quad (8)$$

In general, a, b, c , and d are complex helicity couplings, however several of them vanish for specific groups: $c = d = 0$ for group II ; $b = c = d = 0$ for group III ; and $b = d = 0$ for group IV . There are three special cases for low J^P where additional helicity couplings vanish due to the requirement $|\lambda_1 - \lambda_2| \leq J$: 0^+ in group I , for which $a = c = 0$; 0^- in group II with $a = 0$; and 1^+ in group IV with $c = 0$.

The helicity matrices of different groups are orthogonal to each other given the scalar product

$$(H_1 \cdot H_2) = \text{Tr}(H_1 H_2^\dagger). \quad (9)$$

They produce generally different angular distributions except for a few degenerate cases discussed below. The scalar product in Eq. (9) is used to fix the normalization of H and gives the relation between the helicity couplings:

$$(H \cdot H) = 4|a|^2 + 2|b|^2 + 2|c|^2 + |d|^2 = 1. \quad (10)$$

The form of the helicity matrices in Eq. (7) immediately leads to the conclusion of the Landau-Yang theorem [53, 54]. For the decay of X to a pair of real photons, $H_{0, \lambda} = H_{\lambda, 0} = 0$, as the photon cannot carry the longitudinal polarization, $\lambda = 0$. Practically, this corresponds to setting to zero the second row and second column of the helicity matrix. The matrix of group III completely vanishes, hence, mesons with odd-natural J^P cannot decay to two real photons. The special case of group IV with $c = 0$ also vanishes so the decay of $J^P = 1^+$ to two real photons is also forbidden.

TABLE I: Possible quantum numbers of the decaying particle X separated into four groups with respect to the symmetry of the helicity matrix. The framed quantum numbers in the last column have additional restrictions due to the maximal value of the spin projection.

group	signum $s = (-1)^J$	naturality, $\epsilon = P(-1)^J$	explicit J^P
<i>I</i>	even(+)	natural(+)	0^+ , 2^+ , 4^+ , 6^+
<i>II</i>	even(+)	unnatural(-)	0^- , 2^- , 4^- , 6^-
<i>III</i>	odd(-)	natural(+)	1^- , 3^- , 5^- , 7^-
<i>IV</i>	odd(-)	unnatural(-)	1^+ , 3^+ , 5^+ , 7^+

C. Angular modulations

It is often convenient to simplify the problem and consider only observables that are insensitive to the initial polarization. Once the decay plane orientation is integrated over in Eq. (1), the production polarization matrix R collapses to its trace. Indeed, using the properties of the Wigner D-function and the normalization of R , $\text{Tr } R = 1$ we find that

$$I(\theta_1, \theta_2, \Delta\phi) = \int \frac{d\Omega d\phi_1}{8\pi^2} I(\Omega, \Omega_1, \Omega_2) \quad (11)$$

$$= \sum_{\nu=-2}^2 \sum_{\xi_1, \xi_2}^{\{-1, 1\}} |A_{\xi_1, \xi_2}^\nu(\theta_1, \theta_2, \Delta\phi)|^2.$$

This intensity is a polynomial on trigonometric functions of the angles with the coefficients determined by the helicity couplings. For practical convenience we provide an explicit form of this expression calculated for the general matrix H :

$$I(\theta_1, \theta_2, \Delta\phi) = \sum_{i=1}^6 c_i f_i(\theta_1, \theta_2, \Delta\phi) \quad (12)$$

where f_i are normalized angular functions and c_i are coefficients that depend on the helicity couplings. The functional forms for f_i and c_i are given in Table II.

There are potential cases where different hypotheses are not distinguishable. If a is the only non-zero helicity coupling, the values of ϵ and s enter the angular coefficients c_2 as the product ϵs , and therefore group-*I* has the same angular distributions as group-*IV*, while group-*II* is indistinguishable from group-*III*. Such vanishing of the helicity couplings, however, is an exceptional case and might indicate some other symmetry or additional selection rule.

One dimensional projections or moments can access the same quantities as can be seen from Eq. (12) and Table II. Integrating the intensity over $\cos\theta_1$ and $\cos\theta_2$, the distribution of $\Delta\phi$ is given by

$$I(\Delta\phi) = 1 + \beta \cos(2\Delta\phi), \quad (13)$$

where $\beta = \frac{1}{2}\epsilon|b|^2/(4|a|^2 + 2|b|^2 + 2|c|^2 + |d|^2)$. For odd spins $\beta = 0$, while for even spins, the sign of the $\cos(2\Delta\phi)$

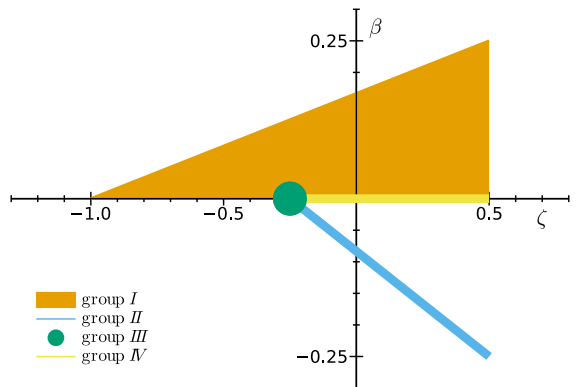


FIG. 3: Allowed values of the angular modulations, β and ζ for the four spin-parity groups in the decays $X \rightarrow 4\mu$.

component is given by the parity. The one-dimensional projection in $\cos\theta_i$, $i = 1, 2$ also provides useful information on the helicity couplings:

$$I(\cos\theta_i) = 1 + \zeta \frac{3 \cos^2\theta_i - 1}{2}, \quad i = 1, 2. \quad (14)$$

with $\zeta = (|b|^2 + |c|^2 - |a|^2 - |d|^2)/(4|a|^2 + 2|b|^2 + 2|c|^2 + |d|^2)$. The value of ζ always falls into the range $[-1, 1/2]$. Furthermore, $\zeta \geq -1/4$ for groups *II* and *IV* while it must be equal to $-1/4$ for group *III*. Fig. 3 summarizes the values possible for β and ζ separated by group.

The idealistic situation of a single isolated resonance discussed so far is, however, rarely achieved in practice: resonances are usually produced superimposed on a continuum distribution or in the presence of additional states. Moreover, interference effects modify the values of the angular asymmetries, β and ζ . In such multicomponent production processes, considerations of both the mass and decay angles of the system are essential to separate the different components. The helicity matrix is modified to take into account the mass dependence of each component. For a given spin J and parity P , it is described by

$$H_{\lambda_1 \lambda_2}^{J^P}(m) = \sum_r H_{\lambda_1 \lambda_2}^{J^P, r} \mathcal{F}_r^{J^P}(m), \quad (15)$$

TABLE II: Basis functions and coefficients for the three-dimensional angular distribution $I(\theta_1, \theta_2, \Delta\phi)$ as expressed in Eq. (12) for final states consisting of four leptons or four scalar particles.

i	angular functions, f_i	coeff. c_i for $X \rightarrow V(l^+l^-)V(l^+l^-)$
1	$9 \sin^2(\theta_1) \sin^2(\theta_2) \sin^2(\Delta\phi)/2$	$-\epsilon b ^2/2$
2	$\sin(\theta_1) \sin(\theta_2) \cos(\theta_1) \cos(\theta_2) \cos(\Delta\phi)$	$(9(\epsilon+1)\text{Re}(b^*d) - 18\epsilon a ^2s)/4$
3	$9 \sin^2(\theta_1) \sin^2(\theta_2)/4$	$(2\epsilon b ^2 - 8 a ^2 + 2 b ^2 + 2 c ^2 + 4 d ^2)/4$
4	$3 \sin^2(\theta_1)/2$	$(6 a ^2 - 3(b ^2 + c ^2))/2$
5	$3 \sin^2(\theta_2)/2$	$(6 a ^2 - 3(b ^2 + c ^2))/2$
6	1	$9(b ^2 + c ^2)/2$

where $H_{\lambda_1\lambda_2}^{J^P,r}$ is a matrix of the complex coupling parameters for the component r having spin J and parity P , m is the mass, and $\mathcal{F}_r^{J^P}(m)$ is its lineshape function. The resonance components have a pole in their parametrization leading to a fast variation of the complex phase in R_π , while the continuum production often follows a power law with slowly moving complex phase.

The amplitude factor that contributes to the intensity

$$\begin{aligned}
 B(m) &= \sum_{j \in \{J^P\}} \epsilon_j \left| \sum_r b^{r,j} \mathcal{F}_r^j(m) \right|^2, \\
 C(m) &= 2 \sum_{j \in \{J^P\}} \left| \sum_r b^{j,r} \mathcal{F}_r^j(m) \right|^2 + 2 \sum_{j \in \{J^P\}} \left| \sum_r c^{j,r} \mathcal{F}_r^j(m) \right|^2 - 2 \sum_{j \in \{J^P\}} \left| \sum_r a^{j,r} \mathcal{F}_r^j(m) \right|^2 - 2 \sum_{j \in \{J^P\}} \left| \sum_r d^{j,r} \mathcal{F}_r^j(m) \right|^2, \\
 D(m) &= 4 \sum_{j \in \{J^P\}} \left| \sum_r a^{j,r} \mathcal{F}_r^j(m) \right|^2 + 2 \sum_{j \in \{J^P\}} \left| \sum_r b^{j,r} \mathcal{F}_r^j(m) \right|^2 + 2 \sum_{j \in \{J^P\}} \left| \sum_r c^{j,r} \mathcal{F}_r^j(m) \right|^2 + \sum_{j \in \{J^P\}} \left| \sum_r d^{j,r} \mathcal{F}_r^j(m) \right|^2,
 \end{aligned} \tag{16}$$

where the summation index j counts all unique J^P assignments and the index r sums over those contributions with that given J^P . The elements of the helicity matrix $H^{j,r}$ are denoted by $b^{j,r}$, $c^{j,r}$, $a^{j,r}$, $d^{j,r}$ according to Eq. (6).

The expression for $D(m)$ describes the total mass spectrum, which, depending on the resonances present and their interference, may show peaking structures above or dips below the continuum. The presence of narrow peaking structures are often taken as evidence for the presence of resonances.

The angular distributions $\beta(m)$ and $\zeta(m)$ present different projections of the intensity. For the continuum, these will vary slowly as a function of mass. They may even be constant if the relative J^P components and components of the helicity matrix do not change with mass. On the pole of a given resonance, it might be expected that β and ζ give the values described above for isolated resonances, and if the resonance does not interfere with the continuum, then the observed value for β or ζ on the

in Eq. 1 must be summed over contributions with spins and parity, and the intensity now has a mass dependence. The angular asymmetries β and ζ in the general case are given by the sum of all components, where the terms with different quantum numbers are added incoherently. β and ζ now depend on mass with $\beta(m) = B(m)/D(m)$ and $\zeta = C(m)/D(m)$ where

pole will add to the value for the continuum and could be used to determine which spin-parity group the resonance belongs to. However, in general this is not true and knowledge is required of the helicity structure of the continuum and its interference with the resonances. However despite this limitation, it should be noted that if a resonance is present, the complex phase varies rapidly around the pole and this will often result in distributions for $\beta(m)$ and $\zeta(m)$ that also vary rapidly with mass. This could be considered as evidence for the presence of resonances, in the same way that variations in the mass spectrum $D(m)$ do, and may help resolve ambiguities.

III. APPLICATION

A. Spin analysis of an isolated resonance

The determination of spin and parity of an isolated resonance is demonstrated using simulated data for the

decay of the Higgs boson. The form of the helicity matrix is found by considering the interaction term of the Higgs with the gauge bosons. The covariant amplitude for $H \rightarrow ZZ$ reads:

$$i\mathcal{M}^{H \rightarrow ZZ} = 2i \frac{m_Z^2}{v} (\varepsilon_1^* \cdot \varepsilon_2^*), \quad (17)$$

where m_Z is the mass of the Z boson and v is the vacuum expectation value of the Higgs field. Using the explicit expressions for the polarization $\varepsilon_i(\lambda_i)$ vectors (see Appendix B), the special form of the matrix for group I is

$$H^{H \rightarrow ZZ} = \frac{1}{\sqrt{3}} \begin{pmatrix} 1 & & \\ & -1 & \\ & & 1 \end{pmatrix} + O(p^2/m_Z^2), \quad (18)$$

where $p = \sqrt{m_H^2 - 4m_Z^2}$ is the break-up momentum of the Z boson in the rest frame of the Higgs boson. The identity matrix corresponds to the S -wave in the decay, while the D -wave is proportional to p^2 and is suppressed at the ZZ threshold. Furthermore, since one Z must be virtual, there is a negligible contribution from the D wave. In the tests presented here, we consider the decay channel $H \rightarrow Z(e^+e^-)Z(\mu^+\mu^-)$; for Z -boson decays to identical final states, the interference between the two decay chains must be included.

A sample of 500 simulated $J^P = 0^+$ events, corresponding to the helicity matrix in Eq. (18), were generated using a dedicated framework written in `Julia` [55]. Results from an analysis using the one-dimensional distributions given in Eq. (13) and (14) are shown in Fig. 4. Superimposed are the theoretical distributions expected from $J^P = 0^+, 0^-$ and 1^- ; the data agree best with the 0^+ hypothesis with the values $\beta_H = 1/6$ and $\zeta_H = 0$. An ensemble of pseudoexperiments lead to estimations for β and ζ that are shown as inset plots and compared to the theoretical values for three spin hypotheses. The width of the distributions indicate the precision of the determination. The 0^+ and 1^- hypotheses are separated by about 2σ , while in the multidimensional approach the statistical significance is about 3.5σ . This shows the improvement in experimental precision that can be achieved by taking account of correlations between the angular variables. Details on hypothesis testing are presented in Appendix C.

B. Structure of the $J/\psi J/\psi$ system

Examination of angular distributions can improve the understanding of the constituents of a mass spectrum, since with multiple interfering components the situation is often unclear. A typical example is the observation by LHCb [13], later confirmed by ATLAS [19] and CMS [20], of structure in the $J/\psi J/\psi$ system that can be interpreted in several ways. At LHCb, two models that have been used to fit the data consider: firstly, one $T_{cc\bar{c}\bar{c}}(6900)$

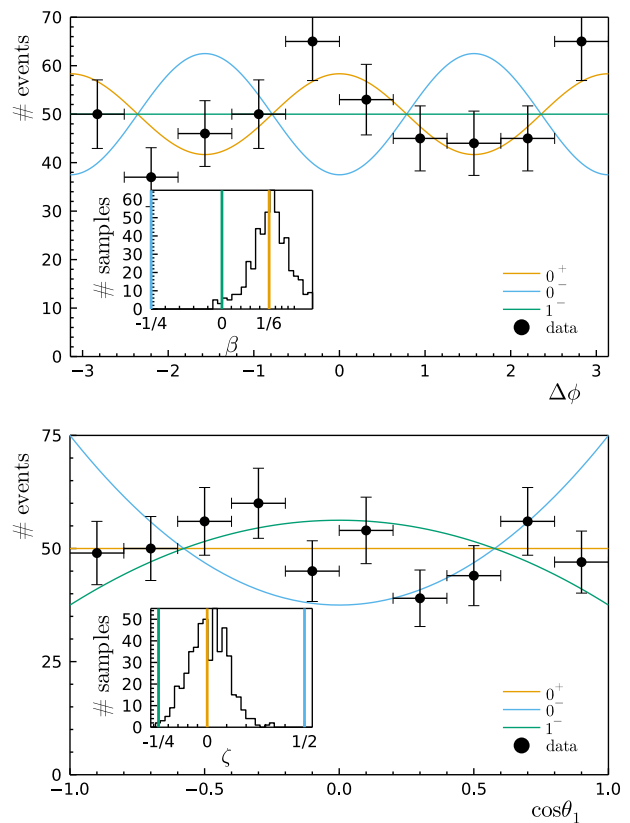


FIG. 4: Distribution of the azimuthal angles $\Delta\phi$ (top) and $\cos\theta_1$ (bottom) for the Higgs decay to $e^+e^-\mu^+\mu^-$ with a single sample of 500 simulated events generated with the $J^P = 0^+$ hypothesis. The orange lines are the expectation curves under the $J^P = 0^+$ hypotheses with $b = d = 1/\sqrt{3}$. The blue lines give the expected dependence for the quantum numbers $J^P = 0^-$ (group II). The distributions for $J^P = 1^-$ are shown by the green lines. The inset plots show distribution of the parameters β and ζ for an ensemble of pseudoexperiments. The coloured lines indicate the true values corresponding to each hypothesis.

resonance and two additional resonances above threshold that do not interfere with the continuum; secondly, one $T_{cc\bar{c}\bar{c}}(6900)$ resonance that does not interfere with the continuum, and another broader resonance that might interfere. We make a qualitative description of experimental spectrum in both models using an exponential function to describe the continuum and Breit-Wigner functions for the resonances. The parameters used are given in Table III and the results are shown in Fig. 5.

The mass distributions are qualitatively similar and with this information alone it is difficult to distinguish between the two competing scenarios. However, the angular distributions allow different structure to be resolved. Far from the resonances the expected values of β and ζ are determined for the continuum. On the peaks of the resonances, deviations from these values are observed, although the nominal values expected for a pure resonance are not achieved due to an admixture of, and possible in-

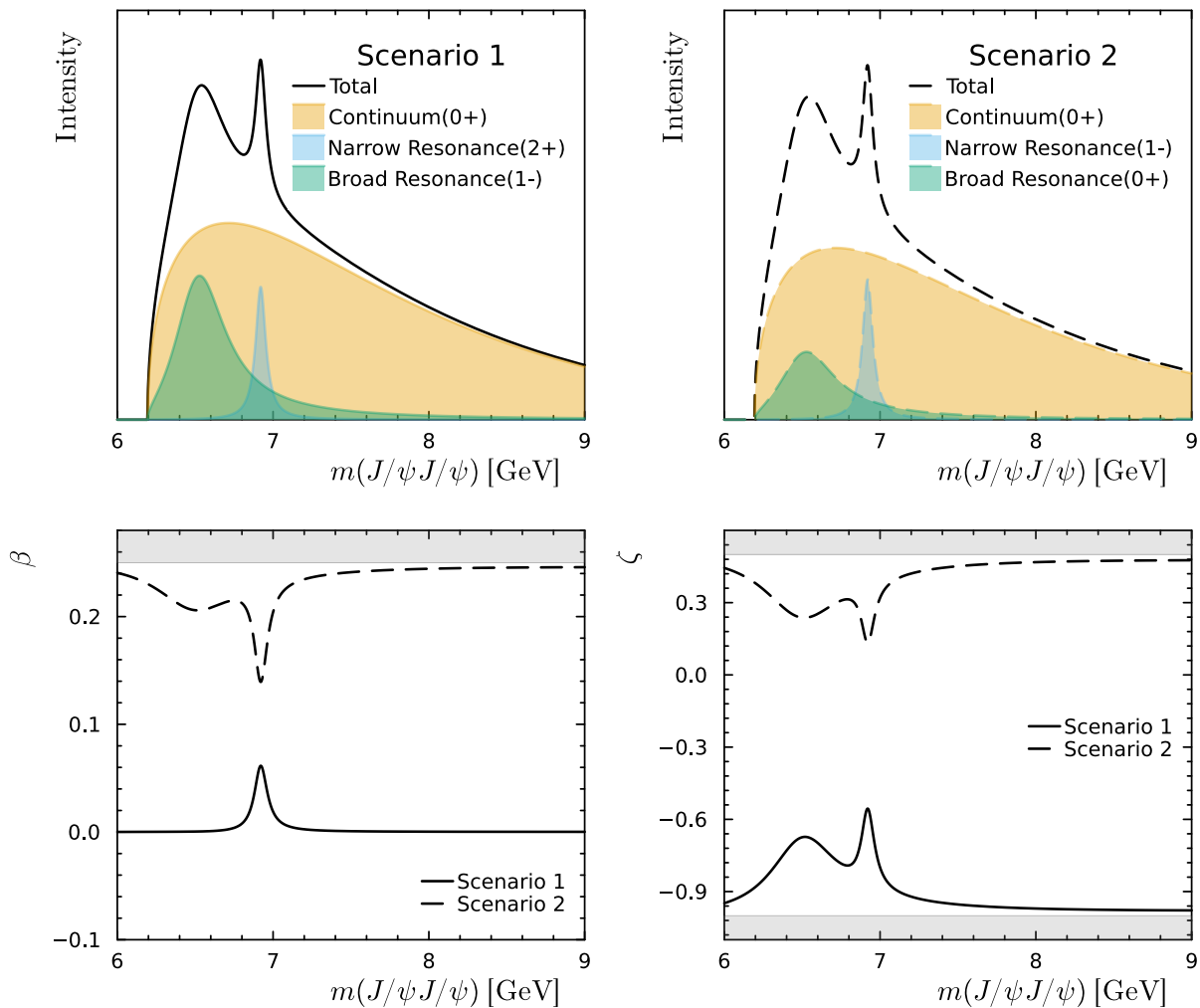


FIG. 5: Top row: Intensity distributions for the two scenarios detailed in Table III. Bottom row: The angular distributions for β (left) and ζ (right) for each scenario.

interference with, the continuum. The structures in the angular distributions are correlated with those in the mass distributions and have widths related to the widths of the resonances. In summary, the angular distributions provide different projections of the amplitude and in some cases may be sufficient to distinguish between different hypotheses, or assist with identification of the spin and parity of putative states.

IV. CONCLUSIONS

A framework has been presented for analysing resonances decaying into two identical vector mesons. In the absence of information on the production polarization, the angular distributions for the decays are fully described through three decay angles. Projections of these enable the decays to be characterised by two parameters, β and ζ whose allowed values can be subdivided

into four groups reflecting the J^P of the parent. Two examples of the use of this formalism were presented: one concerns the Higgs decays to ZZ pairs; the other presents unknown resonances decaying to pairs of J/ψ mesons. The latter is an example of a frequent problem in spectroscopy when trying to determine the presence and quantum numbers of new resonances: consideration of the angular distributions can significantly aid in understanding the underlying physics. We hope this work equips experimental groups with the tools required to incorporate angular distributions into their analyses and we encourage experiments to publish angular information for the decay products along with the mass distributions.

Acknowledgement

The project was motivated by a discussion in the LHCb Amplitude Analysis group. We thank Biplab Dey for

TABLE III: Model parameters used to simulate the $J/\psi J/\psi$ spectrum in two scenarios. For helicity couplings, only non-zero elements are listed. The resonance amplitude is parametrized by the Breit-Wigner formula, $m_0\Gamma_0/(m_0^2 - m^2 - im_0\Gamma_0)$. The exponential shape, $e^{-\beta m}/u$ is used for the continuum, with the factor u ensuring unit integral in the range below 3 GeV above the threshold, $u = \beta(e^{3\beta} - 1)e^{2m_{j/\psi}}$.

	Scenario 1	Scenario 2
Continuum	Exponential	
Slope, β	0.425	
J^P	0^+	0^+
Helicity couplings	$d = 1$	$b = 1/\sqrt{2}$
Normalization	0.2	0.2
Resonance 1	Breit-Wigner	
Mass, m_0	6920 MeV	
Width, Γ_0	80 MeV	
J^P	2^+	1^-
Helicity couplings	$b = d = 1$	$a = 1/2$
Normalization	2	2.2
Resonance 2	Breit-Wigner	
J^P	1^-	0^+
Helicity couplings	$a = 1/2$	$b = 0.3i, d = 0.9$
Mass, m_0	6500 MeV	6492 MeV
Width, Γ_0	400 MeV	450 MeV
Normalization	2.5	1.84

organizing a meeting dedicated to $X \rightarrow VV$. We would like to thank Alessandro Pilloni for useful comments on the work.

Appendix A: Modifications for $X \rightarrow V(S^+S^-)V(S^+S^-)$

The amplitude requires a small modification when a system of four scalar particles is considered, e.g. $\rho(\pi^+\pi^-)\rho(\pi^+\pi^-)$ and $\phi(K^+K^-)\phi(K^+K^-)$. The decay matrix element in Eq. (2) reads:

$$A_{4S}^\nu(\theta_1, \theta_2, \Delta\phi) = 3 \sum_{\lambda_1, \lambda_2} \delta_{\nu, \lambda_1 - \lambda_2} H_{\lambda_1 \lambda_2} d_{\lambda_1, 0}^1(\theta_1) d_{\lambda_2, 0}^1(\theta_2) e^{i\lambda_2 \Delta\phi} \quad (\text{A1})$$

where the decay $V \rightarrow S^+S^-$ proceeds in P -wave only. The functional forms for the three-dimensional angular distribution are given in Table IV. The variation in the $\Delta\phi$ -dependence and $\cos\theta_1$ is more pronounced since there is no averaging over the spins of the final-state particles,

$$\beta_{(S)} = 4\beta_{(l)} = \frac{2\epsilon|b|^2}{4|a|^2 + 2|b|^2 + 2|c|^2 + |d|^2}, \quad \zeta_{(S)} = -2\zeta_{(l)} = \frac{-2|b|^2 - 2|c|^2 + 2|a|^2 + 2|d|^2}{4|a|^2 + 2|b|^2 + 2|c|^2 + |d|^2}, \quad (\text{A2})$$

with lower indices of (S) and (l) to indicate scalar and lepton particles, respectively. The correlation of the β and ζ observables for different groups are shown in Fig. 6.

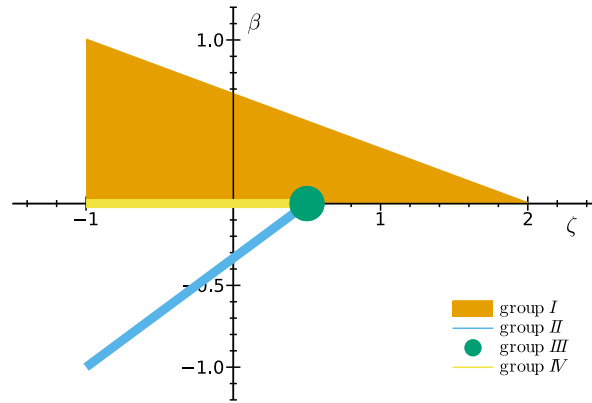


FIG. 6: Allowed values of the angular modulations, β and ζ , for the four spin-parity groups in the decay of X to four scalars.

TABLE IV: Basis functions and coefficients for the three-dimensional angular distribution $I(\theta_1, \theta_2, \Delta\phi)$ as expressed in Eq. (12) for final states consisting of four leptons or four scalar particles.

i	angular functions, f_i	coeff. c_i , for $X \rightarrow V(S^+S^-)V(S^+S^-)$
1	$9 \sin^2(\theta_1) \sin^2(\theta_2) \sin^2(\Delta\phi)/2$	$-2\epsilon b ^2$
2	$\sin(\theta_1) \sin(\theta_2) \cos(\theta_1) \cos(\theta_2) \cos(\Delta\phi)$	$9(\epsilon + 1)\text{Re}(b^*d) - 18\epsilon a ^2s$
3	$9 \sin^2(\theta_1) \sin^2(\theta_2)/4$	$2\epsilon b ^2 - 8 a ^2 + 2 b ^2 + 2 c ^2 + 4 d ^2$
4	$3 \sin^2(\theta_1)/2$	$6 a ^2 - 6 d ^2$
5	$3 \sin^2(\theta_2)/2$	$6 a ^2 - 6 d ^2$
6	1	$9 d ^2$

Appendix B: Polarization vectors

To translate the covariant expression in Eq. (17) to a helicity amplitude, the explicit expressions for the polarization vectors are used:

$$\epsilon_z^\mu(\pm 1) = \frac{1}{\sqrt{2}} (0, \mp 1, -i, 0), \quad \epsilon_z^\mu(0) = \frac{1}{m_Z} (p, 0, 0, E), \quad (\text{B1})$$

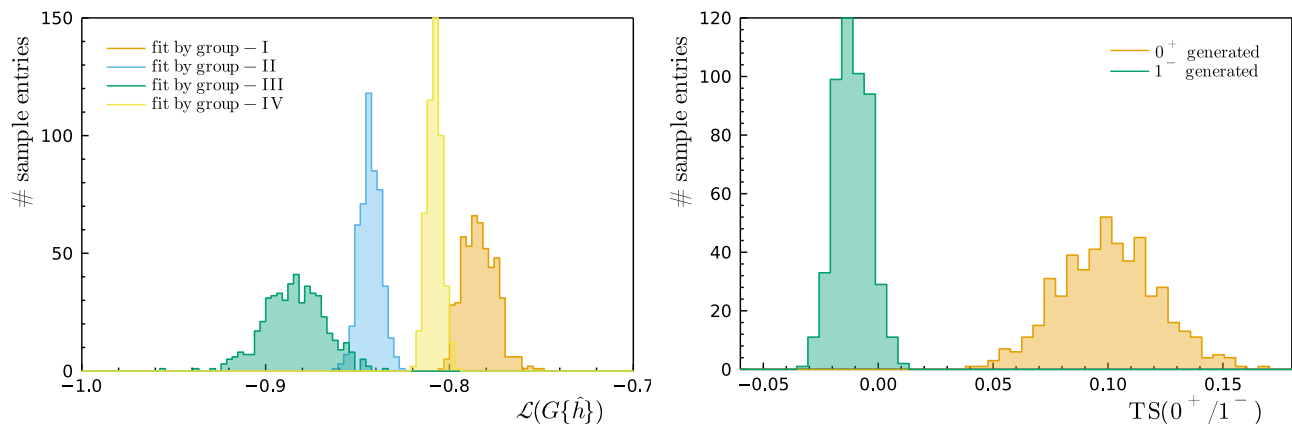


FIG. 7: Left: Distribution of the maximized log-likelihood functions in a series of pseudoexperiments, each of which consists of 500 generated $H \rightarrow Z(e^+e^-)Z(\mu^+\mu^-)$ decays. Right: Distribution of the test statistic $\text{TS}(0^+/1^-)$ for two hypotheses, $J^P = 0^+$ and $J^P = 1^-$, in two sets of pseudoexperiments.

where E , p , and m_Z are the energy, momentum, and mass of the Z boson, respectively. The general expressions for the rotational vectors follow:

$$\varepsilon_1(\lambda) = R_z(\phi)R_y(\theta)\varepsilon_z(\lambda), \quad (\text{B2})$$

$$\varepsilon_2(\lambda) = (-1)^{1-\lambda}R_z(\phi)R_y(\theta)R_y(\pi)\varepsilon_z(\lambda), \quad (\text{B3})$$

where $R_y(\phi)R_y(\theta)$ is a product of the three-dimensional rotation matrices that transforms the vector $(0, 0, 1)$ to the direction $(\sin\theta\cos\phi, \sin\theta\sin\phi, \cos\theta)$. The second particle obtains an additional rotation by π about the y axis since we use the particle-2 phase convention.

Appendix C: Testing hypotheses

Given a set of data corresponding to the decay of particle X , the questions arises as to how well its spin and parity can be determined using the angular distributions. The most powerful method for testing a spin-parity hypotheses is a multidimensional fit, which takes into account the correlations between the angular variables. We confine ourselves here to a three dimensional analysis removing the polarization degrees of freedom, although the discussion can be generalized to the full six-dimensional space treating the polarization as model parameters. To determine which group the particle belongs to, we define a test statistic

$$\text{TS}_{G/G'} = \mathcal{L}_G - \mathcal{L}_{G'}, \quad (\text{C1})$$

where \mathcal{L}_G is the maximized value of the averaged log likelihood for group G and is given by

$$\mathcal{L}_G = \frac{1}{N} \sum_{e=1}^N \log I((\theta_1, \theta_2, \Delta\phi)_e | G\{\hat{h}\}) \quad (\text{C2})$$

where the sum runs over the N events in the sample. The intensity is calculated for each event, assuming it belongs to group G with the helicity couplings \hat{h} that maximize the likelihood.

Distributions of the test statistic in pseudoexperiments is shown in Fig. 7, together with a distribution of the likelihood values for different hypotheses.

-
- [1] M. Gell-Mann, Phys. Lett. **8**, 214 (1964).
 - [2] S. Godfrey and N. Isgur, Phys. Rev. D **32**, 189 (1985).
 - [3] E. Klempt and A. Zaitsev, Phys. Rept. **454**, 1 (2007), 0708.4016.
 - [4] C. Meyer and E. Swanson, Prog. Part. Nucl. Phys. **82**, 21 (2015), 1502.07276.

- [5] S. L. Olsen, T. Skwarnicki, and D. Zieminska, *Rev. Mod. Phys.* **90**, 015003 (2018), 1708.04012.
- [6] N. Brambilla, S. Eidelman, C. Hanhart, A. Nefediev, C.-P. Shen, C. E. Thomas, A. Vairo, and C.-Z. Yuan, *Phys. Rept.* **873**, 1 (2020), 1907.07583.
- [7] S. Godfrey and S. L. Olsen, *Ann. Rev. Nucl. Part. Sci.* **58**, 51 (2008), 0801.3867.
- [8] R. Aaij et al. (LHCb), *Phys. Rev. Lett.* **115**, 072001 (2015), 1507.03414.
- [9] R. Aaij et al. (LHCb), *Phys. Rev. Lett.* **122**, 222001 (2019), 1904.03947.
- [10] F.-K. Guo, C. Hanhart, U.-G. Meißner, Q. Wang, Q. Zhao, and B.-S. Zou, *Rev. Mod. Phys.* **90**, 015004 (2018), [Erratum: *Rev.Mod.Phys.* 94, 029901 (2022)], 1705.00141.
- [11] R. Aaij et al. (LHCb), *Phys. Rev. Lett.* **125**, 242001 (2020), 2009.00025.
- [12] R. Aaij et al. (LHCb), *Phys. Rev. D* **102**, 112003 (2020), 2009.00026.
- [13] R. Aaij et al. (LHCb), *Sci. Bull.* **65**, 1983 (2020), 2006.16957.
- [14] R. Aaij et al. (LHCb), *Phys. Rev. Lett.* **131**, 041902 (2023), 2212.02716.
- [15] R. Aaij et al. (LHCb), *Phys. Rev. D* **108**, 012017 (2023), 2212.02717.
- [16] R. Aaij et al. (LHCb), *Nature Phys.* **18**, 751 (2022), 2109.01038.
- [17] R. Aaij et al. (LHCb), *Nature Commun.* **13**, 3351 (2022), 2109.01056.
- [18] M. Jacob and G. Wick, *Annals Phys.* **7**, 404 (1959).
- [19] G. Aad et al. (ATLAS), *Phys. Rev. Lett.* **131**, 151902 (2023), 2304.08962.
- [20] A. Hayrapetyan et al. (CMS), *Phys. Rev. Lett.* **132**, 111901 (2024), 2306.07164.
- [21] X.-K. Dong, V. Baru, F.-K. Guo, C. Hanhart, and A. Nefediev, *Phys. Rev. Lett.* **126**, 132001 (2021), [Erratum: *Phys.Rev.Lett.* 127, 119901 (2021)], 2009.07795.
- [22] J.-Z. Wang, D.-Y. Chen, X. Liu, and T. Matsuki, *Phys. Rev. D* **103**, 071503 (2021), 2008.07430.
- [23] M. Karliner and J. L. Rosner, *Phys. Rev. D* **102**, 114039 (2020), 2009.04429.
- [24] C. Gong, M.-C. Du, Q. Zhao, X.-H. Zhong, and B. Zhou, *Phys. Lett. B* **824**, 136794 (2022), 2011.11374.
- [25] Y.-R. Liu, H.-X. Chen, W. Chen, X. Liu, and S.-L. Zhu, *Prog. Part. Nucl. Phys.* **107**, 237 (2019), 1903.11976.
- [26] X.-Z. Weng, X.-L. Chen, W.-Z. Deng, and S.-L. Zhu, *Phys. Rev. D* **103**, 034001 (2021), 2010.05163.
- [27] H.-X. Chen, W. Chen, X. Liu, and S.-L. Zhu, *Sci. Bull.* **65**, 1994 (2020), 2006.16027.
- [28] H.-T. An, S.-Q. Luo, Z.-W. Liu, and X. Liu (2022), 2208.03899.
- [29] C. Becchi, J. Ferretti, A. Giachino, L. Maiani, and E. Santopinto, *Phys. Lett. B* **811**, 135952 (2020), 2006.14388.
- [30] T. Armstrong et al. (WA76), *Phys. Lett. B* **228**, 536 (1989).
- [31] S. Abatzis et al. (WA91), *Phys. Lett. B* **324**, 509 (1994).
- [32] K. Österberg (TOTEM), *Int. J. Mod. Phys. A* **29**, 1446019 (2014).
- [33] D. Barberis et al. (WA102), *Phys. Lett. B* **474**, 423 (2000), hep-ex/0001017.
- [34] P. Lebiedowicz, O. Nachtmann, and A. Szczurek, *Phys. Rev. D* **99**, 094034 (2019), 1901.11490.
- [35] N.-P. Chang and C. Nelson, *Phys. Rev. Lett.* **40**, 1617 (1978).
- [36] T. Trueman, *Phys. Rev. D* **18**, 3423 (1978).
- [37] W.-Y. Keung, I. Low, and J. Shu, *Phys. Rev. Lett.* **101**, 091802 (2008), 0806.2864.
- [38] Y. Gao, A. V. Gribsan, Z. Guo, K. Melnikov, M. Schulze, and N. V. Tran, *Phys. Rev. D* **81**, 075022 (2010), 1001.3396.
- [39] S. Bolognesi, Y. Gao, A. V. Gribsan, K. Melnikov, M. Schulze, N. V. Tran, and A. Whitbeck, *Phys. Rev. D* **86**, 095031 (2012), 1208.4018.
- [40] T. Modak, D. Sahoo, R. Sinha, H.-Y. Cheng, and T.-C. Yuan, *Chin. Phys. C* **40**, 033002 (2016), 1408.5665.
- [41] S. Berge, S. Groote, J. G. Körner, and L. Kaldamäe, *Phys. Rev. D* **92**, 033001 (2015), 1505.06568.
- [42] K. Gottfried and J. D. Jackson, *Nuovo Cim.* **33**, 309 (1964).
- [43] J. C. Collins and D. E. Soper, *Phys. Rev. D* **16**, 2219 (1977).
- [44] R. Aaij et al. (LHCb), *Eur. Phys. J. C* **73**, 2631 (2013), 1307.6379.
- [45] S. Chatrchyan et al. (CMS), *Phys. Rev. Lett.* **110**, 081802 (2013), 1209.2922.
- [46] T. Aaltonen et al. (CDF), *Phys. Rev. Lett.* **108**, 151802 (2012), 1112.1591.
- [47] R. Aaij et al. (LHCb), *Phys. Lett. B* **724**, 27 (2013), 1302.5578.
- [48] A. M. Sirunyan et al. (CMS), *Phys. Rev. D* **97**, 072010 (2018), 1802.04867.
- [49] R. Pasechnik, A. Szczurek, and O. Teryaev, *Phys. Rev. D* **83**, 074017 (2011), 1008.4325.
- [50] M. Mikhasenko et al. (JPAC), *Phys. Rev. D* **101**, 034033 (2020), 1910.04566.
- [51] A. D. Martin and T. D. Spearman, *Elementary-particle theory* (North-Holland, Amsterdam, 1970), URL <https://cds.cern.ch/record/102663>.
- [52] P. D. B. Collins, *An Introduction to Regge Theory and High-Energy Physics*, Cambridge Monographs on Mathematical Physics (Cambridge Univ. Press, Cambridge, UK, 2009), ISBN 9780521110358, URL <http://www-spires.fnal.gov/spires/find/books/www?cl=QC793.3.R4C695>.
- [53] C.-N. Yang, *Phys. Rev.* **77**, 242 (1950).
- [54] L. Landau, *Dokl. Akad. Nauk SSSR* **60**, 207 (1948).
- [55] *The JpsiJpsi framework implemented in Julia*, Available at <https://github.com/mmikhasenko/JpsiJpsi.jl>.